Experimental and Theoretical Study of Tunable Photonic Crystal Laser Using Liquid Crystal

Ryotaro OZAKI*

Abstract: Liquid crystals are mesophases between crystalline solids and isotropic liquids. Their fluidity and dielectric anisotropy allow molecular reorientation in nano structures. Since the field-induced molecular reorientation gives rise to a change in optical properties, liquid crystal infiltrated photonic crystals have been regarded as potential candidates for tunable photonic crystals. In this paper, fundamentals of photonic crystals are described to explain photonic band structures, photonic bandgaps, and defect modes. A one-dimensional photonic crystal with a liquid crystal defect layer is experimentally studied for application as a tunable laser. Numerical analyses are also carried out to simulate the physical properties: photonic band structures, light propagation, electric-field enhancement, and density of states.

Keywords: Photonic crystal, Liquid crystal

1. Introduction

Liquid crystals are mesophases between crystalline solids and isotropic liquids. They may flow like viscous fluids and also possess features that are characteristic of solid crystals. The constituents are rod-like or disk-like organic molecules which normally have self-assembled characteristics. These molecules exhibit different physical properties between the long and short molecular axes. Owing to their molecular shape, liquid crystals have various anisotropic properties, such as permittivity, refractive index, and viscosity. There are many types of liquid crystal states which are classified by the long-range orientational order of the molecules.[1,2] In a nematic phase, rod-like molecules are aligned to a certain direction but they do not have a positional order. The nematic phase is the most commonly used in flat panel displays.[3,4] This is because nematic liquid crystals have high fluidity and large dielectric anisotropy which are key properties in the liquid crystal devices. Since the fluidity and dielectric anisotropy allow liquid crystal molecules to align parallel to or perpendicular to an electric field, the molecular director can be controlled by application of an electric field. On the basis of this field-induced molecular reorientation, almost all liquid crystal devices act as optical shutters.

Liquid crystal infiltrated photonic crystals have attracted considerable attention from both fundamental and practical points of view, because they can be regarded as tunable photonic crystals.[5-11] Photonic crystals are *one-dimensional (1D), two-dimensional (2D) or three-dimensional (3D) ordered structures with a periodicity comparable to an optical wavelength. They are composed of two or more different dielectrics and their periodicity opens up a photonic bandgap in which the existence of photons is forbidden.[12-15] This can be

* Department of Electrical and Electronic Engineering and Computer Science, Graduate School of Science and Engineering, Ehime University

原稿受理　平成 24 年 10 月 31 日

explained by an analogy to electrons in a solid-state crystal. In a photonic bandgap, electromagnetic fields cannot propagate due to destructive interference between waves scattered from the periodically modulated refractive-index structure. This is similar to destructive interference of electron waves from the periodic potential of an atomic lattice at a certain frequency.

When there is a defect which disturbs the periodicity of a photonic crystal structure, localized photonic states appear in the photonic bandgap. The states are so-called defect modes at which photons are confined in the defect. In particular, 3D photonic bandgap materials with a defect allow us to achieve a 3D photon confinement.[12-13] Such an optical confinement is the most important feature of photonic crystals because the electric field in a defect can be strongly enhanced at a defect mode resonance frequency. An appropriate line defect in a 2D or 3D photonic crystal serves as a waveguide that can guide light in a desired direction by photonic bandgap confinement.[16,17] Such a defect acting as a microcavity or a waveguide is very important in certain applications, for example, low-threshold lasers, micro-waveguides, optical circuits, and so on.[16-22] Furthermore, tunable photonic crystals having variable photonic bandgaps by controlling optical periodicities are also utilized for functional applications, for example, tunable lasers[8-9,23-27] and tunable optical waveguides.[28] In particular, liquid crystal infiltrated photonic crystals have been studied for the realization of tunable photonic crystals. When a liquid crystal is used as a material of a periodic structure, photonic bandgaps can be controlled because liquid crystals have a large optical anisotropy and are sensitive to external conditions such as temperature, electric fields, and magnetic fields. The field-induced molecular reorientation gives rise to a change in the optical length of a photonic crystal. In the cases of opals or inverse opals filled with a nematic liquid crystal, tunable photonic bandgap has been demonstrated by applying an electric field or by controlling temperature.[5,6]

Tunable defect modes are also an attractive subject. However, introduction of defects in a 3D photonic crystal using nano-fabrication remains a major technical challenge.[29-32] Although 1D photonic crystals do not have a complete photonic bandgap, there are plenty of applications using extraordinary wavelength dispersion and a localized photonic state in the defect layer. So far, intensive studies on 1D photonic crystal applications have been reported: air-bridge microcavities,[33,34] photonic band-edge lasers,[20] nonlinear optical diodes,[35] and enhancements of optical nonlinearity.[36,37] In this paper, we focus on a 1D tunable photonic crystal using a liquid crystal and study its application as a tunable laser.

2. Fundamentals of 1D Photonic Crystals

Photonic crystals have photonic bandgaps which forbid electromagnetic wave propagation in a certain direction. Figure 1 shows the schematic views of photonic crystals. Photonic crystals are 1D, 2D or 3D ordered structures with a periodicity comparable to an optical wavelength. They are composed of two or more different dielectrics and their periodicity opens up a photonic bandgap in which the existence of photons is forbidden. To understand optical characteristics of a photonic crystal, photonic band analysis is particularly important. The photonic band diagram of a photonic crystal, which allows the survey of all the dispersion characteristics of the photonic crystal, can be obtained by solving Maxwell's equations directly. There are several numerical methods for photonic band analysis, such as the plane wave expansion (PWE) method[38,39] and the finite-difference time-domain (FDTD) method.[40,41] These methods allow us to calculate not only the photonic band diagram

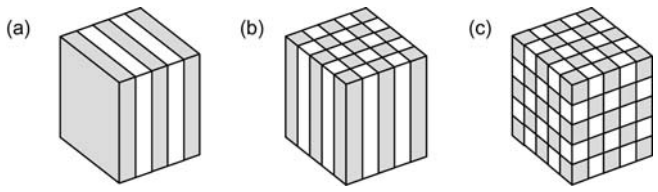

Fig.1 Schematic views of photonic crystals: (a) 1D photonic crystal, (b) 2D photonic crystal, and (3) 3D photonic crystal.

but also electric field profiles in the photonic crystal. Here we discuss some of the basic properties of a 1D photonic crystal using the calculation results.

Figure 2(a) shows the photonic band structure of a 1D photonic crystal calculated by the PWE method with the following parameters: refractive indices $n_1 = 2.35$, $n_2 = 1.45$; layer thickness $L_1 = L_2 = 70$ nm. In Fig. 2(a), the vertical axis represents normalized frequency $\omega a/2\pi c$ and the horizontal axis represents wave vector k, where a is the lattice constant and c is the speed of light. In general, normalized frequency is used as the vertical axis because of the existence of a simple scaling law concerned with the lattice constant and wavelength. In the diagram, there are some gaps in which wave vector does not exist over a certain frequency range. The gaps are the so called photonic bandgaps. To improve understanding of the diagram, Fig. 2(b) shows the transmission spectrum of the 1D photonic crystal calculated by the transfer matrix method.[15] It is clear that the dips in transmittance appear over the frequency ranges of the photonic bandgaps. The diagram also shows small group velocities near the band edges, which is determined by the slope of the curve, i.e. $v_g = d\omega/dk$.

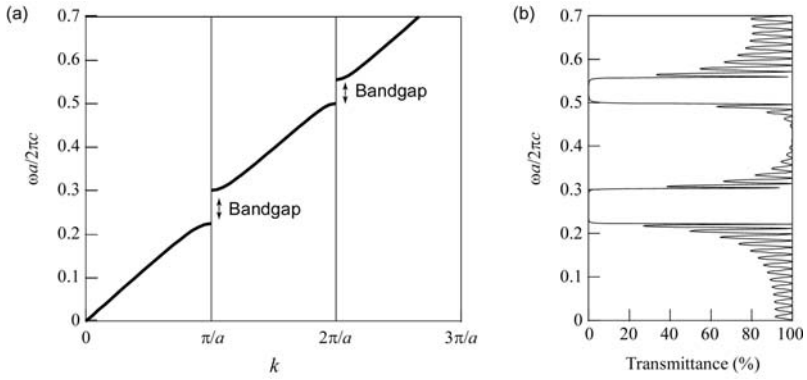

Fig.2 (a) Photonic band structure of the 1D photonic crystal calculated by the PWE method. (b) Transmission spectrum of the 1D photonic crystal calculated by the transfer matrix method. The parameters are as follows: refractive indices $n_1 = 2.35$, $n_2 = 1.45$; layer thickness $L_1 = L_2 = 70$ nm.

Electric field profiles in the 1D photonic crystal for various frequencies are shown in Fig. 3. The electric fields are calculated by the transfer matrix method with the same parameters as the transmission spectrum. Figure 3(a) shows the electric field for $\omega a/2\pi c = 0.15$, where the darker and lighter gray layers represent $n_1 = 2.35$ and $n_2 = 1.45$, respectively. The incident light enters from the left, and then propagates through the 1D photonic crystal without disturbance. This is because the light propagation is hardly affected by the dielectric

periodic structure at the photonic band frequency. The electric field at the bandgap frequency $\omega a/2\pi c = 0.22$ is shown in Fig. 3(b). The incident light exponentially decreases inside the 1D photonic crystal. At this frequency the phases of reflected light from boundaries are matched, and then the in-phase reflections give rise to strong light reflection. Namely, the internal interference forbids the existence of light at the photonic bandgap frequency.

When the light with a photonic band edge frequency enters the 1D photonic crystal, the electric field is enhanced. Figures 3(c) and 3(d) show the electric field profiles at the lower and upper band edge, respectively. Since their group velocities approach zero at the band edges, the electric and magnetic fields form a standing wave in the 1D photonic crystal. At both band edges, the electric field is enhanced because the photonic crystal acts as a resonant cavity. In Fig. 3(c), the peaks of the inside electric field are located on the darker layers. This means that the photons are concentrated in the higher index regions; $n_1 = 2.35$. In contrast, the peaks of the inside electric field in Fig. 3(d) are located on the lighter layers. The refractive index n_2 of the lighter gray layer is 1.45. Since the energy of a photon becomes lower in a higher-index medium, the difference in energy between the lower and upper band edges can be explained by where photons are concentrated. In general, such an electric field enhancement at the band edge is used for a distributed feedback (DFB) laser.

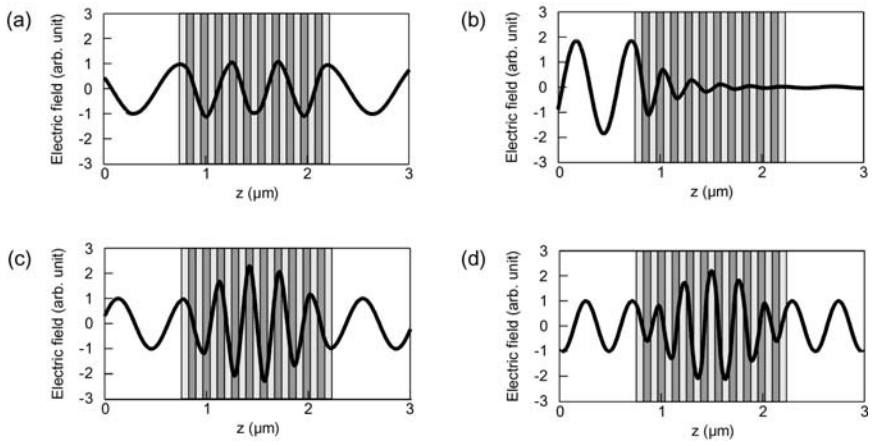

Fig. 3 Electric field profiles in the photonic crystal for various situations: (a) photonic band, (b) photonic bandgap, (c) lower band edge, and (d) upper band edge.

One of the attractive features of photonic crystals is a defect mode in a photonic bandgap. When a defect of periodicity is introduced into the lattice, photons are strongly localized in the defect. Figure 4(a) shows the transmission spectrum of a 1D photonic crystal with an air gap. The following parameters are used: $n_1 = 2.35$, $n_2 = 1.45$, $n_d = 1.0$, $L_1 = 64$ nm, $L_2 = 103$ nm, and $L_d = 75$ nm, where n_d is the refractive index of the air defect and L_d isthe defect length. The photonic bandgap is formed from 510 nm to 780 nm in which the sharp peak appears at 640 nm due to the introduction of the air defect. The narrow peak corresponds to a defect state that is a localized mode in the photonic bandgap. Figure 4(b) shows the electric field profile at the defect mode frequency. It is clear that the electric fields are strongly enhanced in the defect. Note that the peak intensity for the defect mode is larger than those for the band-edge modes shown in Figs. 3(c) and 3(d). The reason is that photons are confined in the narrow defect at the defect mode, whereas photons are confined in the whole photonic crystal at

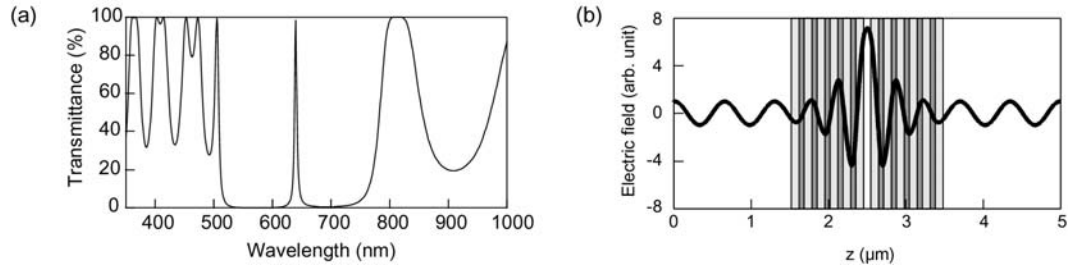

Fig. 4 (a) Transmission spectrum of a 1D photonic crystal with an air defect. (b) Electric field profile at the defect mode wavelength of 640 nm.

the band-edge modes. The electric field enhancement allows strong interactions between photons and materials. Such photonic crystals with a defect are expected to enhance an optical gain, a nonlinear-optical effect, or a magneto-optical effect.

3. Photonic Crystal Lasers

Optical properties of a photonic crystal, such as photonic bandgap and defect mode, depend on the structural periodicity and the refractive indices of the materials. If we can tune the structural periodicity or refractive index in a photonic crystal, the optical properties can be controlled. There are several ways to change the optical periodicity. For example, an external stress will induce a deformation in the periodic structure,[25] and temperature control is also effective for changing the refractive index of a material.[5,6] However, from the standpoint of application to optical devices, the precision and speed of tuning by stress or temperature are inferior compared to an electrical control. Liquid crystals have a large birefringence and their refractive indices can be electrically controlled by molecular reorientation. Therefore, liquid crystal is one of the suitable materials for tunable photonic crystals.

3.1 Tunable Defect Mode

Let us consider a nematic liquid crystal introduced into a 1D photonic crystal, as shown in Fig. 5. The photonic crystal is composed of dielectric multilayers with the nematic liquid crystal defect layer located at the center. We assume that the initial orientation of the liquid crystal molecules is set along the *y*-axis and that the molecules are reoriented parallel to the *z*-axis by applying an electric field. In general, there exists a threshold electric field E_{th} above which the molecules can be redirected from the initial orientation. It is well known that a nematic liquid crystal has such a threshold caused by the Frederiks transition.[1,2] The threshold is given by

$$E_{th} = \frac{\pi}{d}\sqrt{\frac{K_{11}}{\varepsilon_0 \Delta\varepsilon}} \quad , \tag{1}$$

where d is thickness of the liquid crystal layer, K_{11} is the splay elastic constant, ε_0 is the vacuum permittivity, $\Delta\varepsilon$ is dielectric anisotropy of the liquid crystal. The threshold voltage V_{th} is easily obtained from simple calculation and is approximately 1 V for a typical nematic liquid crystal.

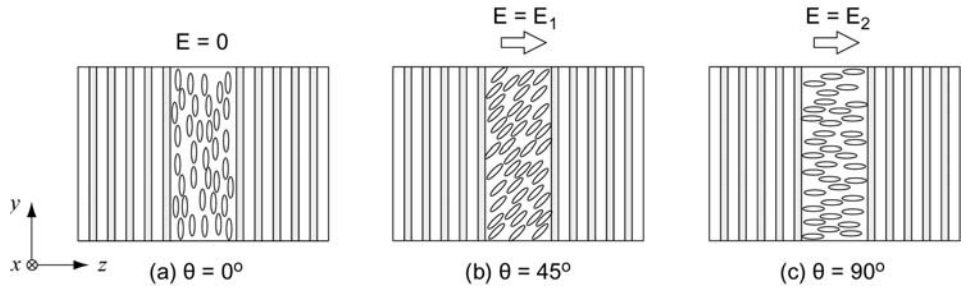

Fig. 5 Schematic views of a 1D photonic crystal with a nematic liquid crystal for (a) E = 0, θ = 0°, (b) E = E_1, θ = 45°, and (c) E = E_2, θ = 90° ($E_2 > E_1 > E_{th}$). The liquid crystal director can be controlled using electric-field-induced molecular reorientation.

When light linearly polarized along the *y*-axis enters a photonic crystal, the incident light encounters the extraordinary refractive index n_e in the liquid crystal layer in the absence of an applied electric field. Above E_{th}, the molecules tilt towards the *z*-axis by an angle θ from the *y*-axis. Using the angle, the effective refractive index $n'(\theta)$ for the *y*-polarization is determined by

$$n'(\theta) = \frac{n_o n_e}{\sqrt{n_e^2 \sin^2\theta + n_o^2 \cos^2\theta}}. \qquad (2)$$

When the molecules are aligned parallel to the *z*-axis by a sufficient voltage, the effective refractive index becomes equal to the ordinary index n_o; $n'(90^o) = n_o$. Since nematic liquid crystals have a large anisotropy in refractive index, the molecular reorientaion in the defect layer gives rise to a change in the optical length. This indicates that the defect mode wavelength can be controlled by applying voltage to the liquid crystal defect layer.

Figure 6 shows the experimental setup for optical transmission measurement. A dielectric multilayer consisting of an alternating stack of SiO_2 and TiO_2 layers deposited on an In-Sn oxide (ITO)-coated glass substrate was used as a 1D photonic crystal. The refractive indices of SiO_2 and TiO_2 are 1.45 and 2.35, respectively. The center wavelength of the photonic band was adjusted to be 600 nm by setting the optical thickness of both SiO_2 and TiO_2 to be one-quarter of 600 nm; the thickness of SiO_2 and TiO_2 layers were 103 nm and 64 nm, respectively. The number of SiO_2-TiO_2 pairs on each substrate was five. Polyimide was spin-coated on the top surface of the multilayer, and then it was unidirectionally rubbed along the *y*-axis. The polyimide

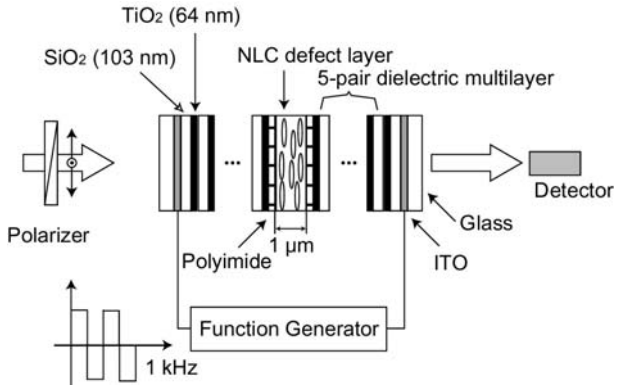

Fig. 6 1D photonic crystal containing a nematic liquid crystal as a defect layer and experimental setup for electrical tuning of the defect mode.

would then align liquid crystal molecules parallel to the *y*-direction. To introduce the defect layer, a nematic liquid crystal was sandwiched between two multilayers using 1-μm spacers. The ordinary and extraordinary refractive indices of the liquid crystal are approximately n_o = 1.5 and n_e = 1.7, respectively. Figure 7(a) shows the experimentally measured transmission spectra of the 1D photonic crystal with a nematic liquid crystal defect layer. The transmission spectra were measured with *y*-polarized light which corresponds to the initial orientation of the liquid crystal molecules in the defect layer. The solid and broken lines represent the transmission spectra at 0 V and 8 V, respectively. An application of a voltage to ITO electrodes changes the molecular alignment of the liquid crystal defect layer. The defect mode peaks shift to the shorter wavelength side upon applying voltage. Figure 7(b) shows the calculated transmission spectra of the 1D photonic crystal with a nematic liquid crystal defect layer. These calculations were carried out using the 4×4 matrix method.[42] This method is a numerical analysis based on the Maxwell equations which can be used to quantitatively calculate the light propagation in an anisotropic medium with refractive index varying along one direction. The peak shifts agree with the calculation results in Fig. 7(b). Namely, the incident light encounters n_e at the initial orientation and then encounters n_o at 8 V. The measured peak widths are broader than the calculated ones due to non-uniformity of the physical thickness of the defect layer.

The voltage dependences of the defect mode wavelengths for the light polarized along the *x*- and the *y*-axes are summarized in Fig. 8. The open and filled circles represent the peak wavelengths for *x*- and *y*-polarizations,

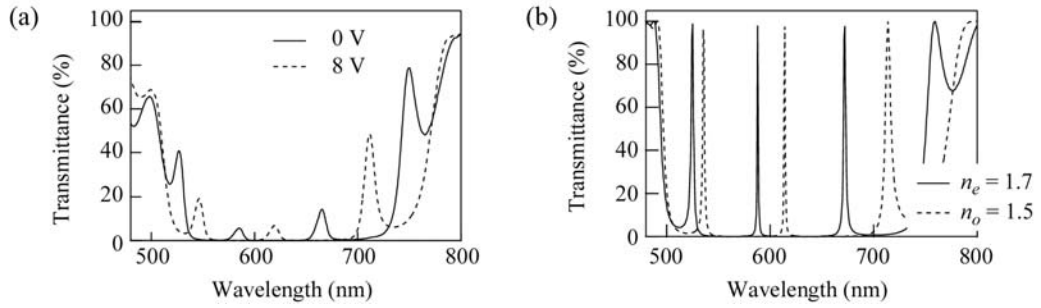

Fig. 7 (a) Experimentally measured transmission spectra of the 1D photonic crystal with a nematic liquid crystal defect layer. (b) Calculated transmission spectra of the photonic crystal by the 4×4 matrix method.

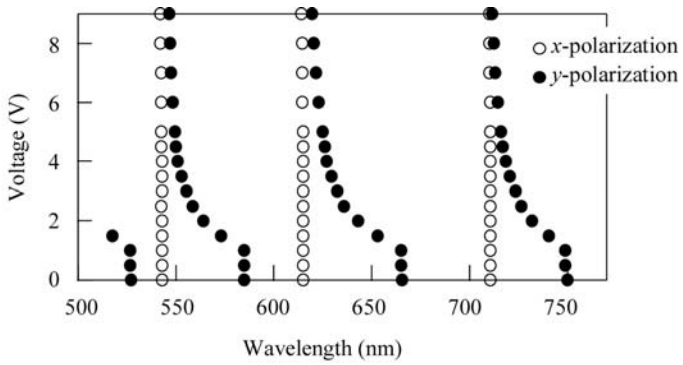

Fig. 8 Voltage dependences of defect mode peaks of the 1D photonic crystal with a nematic liquid crystal. The open and filled circles represent the peak wavelengths for *x*- and *y*-polarizations.

respectively. For *y*-polarized light, the defect mode peaks begin to shift to shorter wavelengths with increasing voltage above 1 V which is associated with the Frederiks transition mentioned above. All peaks shift in the same manner by about 40 nm, even upon applying low voltage. The peak located around 530 nm at 0 V shifts to a shorter wavelength and disappears above 1.8 V, which means that the peak is out of the band gap at higher voltages and is no longer a defect mode. In contrast, the defect modes for *x*-polarized light remains unchanged upon applying voltage. This indicates that the *x*-polarized light is always affected by n_o, regardless of the applied voltage. This is because the *x* component of the refractive index is not changed by the reorientation. Therefore, for *x*-polarized light, the optical length of the defect layer is independent of the liquid crystal molecular orientation.

3.2 Defect Mode Laser

Although 1D photonic crystals do not have a complete photonic bandgap, there are many applications using the slow group velocity at a band edge and the localized photonic state in a defect layer. In particular, the study of defect mode lasing is one of the most attractive subjects because low threshold lasing at a defect mode resonance is expected. Since defect mode wavelengths can be controlled upon applying electric field using a liquid crystal defect, lasing wavelength can also be tuned. Electrically wavelength-tunable defect mode lasing has been demonstrated using this system.[8,43] In the experiments, an active medium was introduced inside the 1D photonic crystal with a liquid crystal defect to achieve laser action. As an active laser medium, a laser dye[8] or a conducting polymer[43] was used. To excite the active medium, the second-harmonic light of a Q-switched Nd:YAG laser irradiated the sample. Figure 9 shows experimental setup for lasing wavelength control upon the applied voltage. In this case, [2-[2-4-(dimethylamino)phenyl]ethenyl]-6-methyl-4H-pyran-4-ylidene propanedinitrile was used as a laser dye dopant in the nematic liquid crystal. Figure 10(a) shows the pump energy dependence of emission intensity at the defect mode wavelength. Above the threshold at a pump-pulse energy of about 5 μJ/pulse, the emission intensity significantly increases. This indicates that there exists a lasing threshold above which a light amplification accrues. In order to control the emission wavelength, the orientation of the liquid crystal molecules in the defect layer was changed upon applying a square-wave voltage at 1 kHz. Figure 10(b) shows the emission spectra of the 1D photonic crystal with the dye-doped liquid crystal defect as a function of applied voltage. It should be noted that a sharp lasing peak shifts toward shorter wavelengths with increasing voltage in the same manner as the defect modes shift (see Fig. 8). The wavelength shift of the lasing peak is about 25 nm, even upon applying low voltage. The lasing in a 1-D photonic crystal with a liquid crystal defect layer can be tuned over a wide range upon applying an electric field.

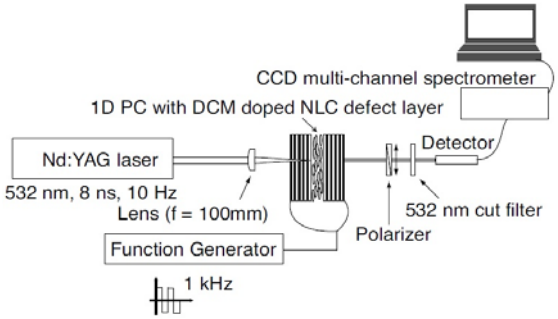

Fig. 9 Experimental setup for lasing wavelength control upon the applied voltage.

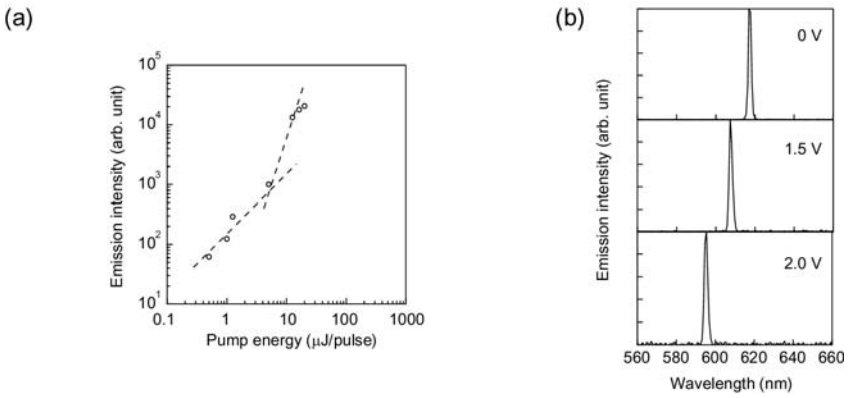

Fig. 10 (a) Pump energy dependence of emission intensity at the defect mode wavelength. (b) Emission spectra of the 1D photonic crystal with dye-doped liquid crystal defect as a function of applied voltage.

3.3 Density of States

The density of states (DOS), which is the reciprocal of the group velocity of light, plays an important role in photonic crystal lasers.[44,45] The photonic DOS $\rho(\omega)$ is defined as the inverse slope of the dispersion relation,

$$\rho(\omega) = \frac{1}{v_g(\omega)} = \frac{dk(\omega)}{d\omega}. \tag{3}$$

As is evident from the equation, a slow group velocity in a photonic crystal provides a large DOS which is the same meaning as strong confinement. The dispersion relation of a photonic crystal can be calculated by the PWE method or other numerical methods. However, these methods can obtain a photonic band diagram for an infinite period but not for a finite period. Here the DOS in a finite periodic structure is calculated with the complex transmission coefficient t written as

$$t = t_1 + it_2 \left(= \frac{E_t}{E_i} \right) \quad , \tag{4}$$

where t_1 and t_2 are the real and imaginary parts of the transmission coefficient, and E_t and E_i are the amplitudes of the transmitted and incident electric fields. Using the complex transmission coefficient, the DOS is given by

$$\rho(\omega) = \frac{dk(\omega)}{d\omega} = \frac{1}{D} \frac{\left(\frac{dt_2}{d\omega}\right) t_1 - \left(\frac{dt_1}{d\omega}\right) t_2}{t_1^2 + t_2^2} \quad , \tag{5}$$

where D is the thickness of the sample. The DOS for an isotropic medium ρ_{iso} is

$$\rho_{iso} = \frac{dk}{d\omega} = \frac{n}{c}. \tag{6}$$

Figure 11(a) shows the transmission spectrum and the normalized DOS of a 10-layer SiO_2-TiO_2 stack without a defect. Here, t_1 and t_2 are calculated using the 4×4 matrix method. The DOS is increased at the band edges because of slow group velocities. We can estimate a lasing wavelength in the DFB cavity from the peak of the DOS. Figure 11(b) shows the transmission spectrum and the normalized DOS of a 10-layer SiO_2-TiO_2 stack with a defect. The defect is sandwiched between two 5-layer stacks, and its refractive index and length are 1.7 and 190 nm, respectively. As is evident from Fig. 11(b), the DOS at the defect mode wavelength is significantly

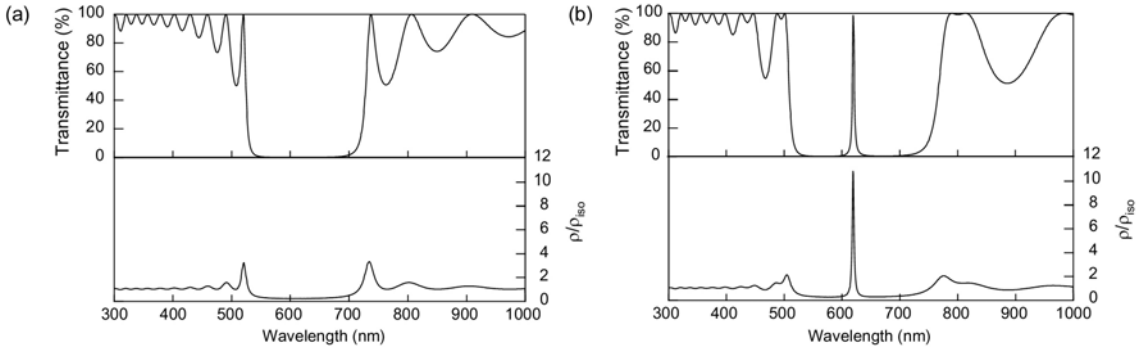

Fig. 11 Transmission spectra and normalized DOSs of a 10-layers SiO_2-TiO_2 multilayer: (a) without a defect and (b) with a defect.

increased. That is, the group velocity at the defect mode wavelength is much slower than that at the band edges. This result is consistent with the electric field calculations shown in Figs. 3 and 4. Such a slow group velocity and an electric field enhancement are major advantages of a defect mode because an electric field can interact more strongly with a functional material in the defect. Thus, the analysis of the DOS is one of the most useful tools to investigate optical confinement in a photonic crystal.

3.4 ADE-FDTD Simulations

The FDTD method also plays an important role in computer-aided analysis for photonic crystal lasers, in which the Maxwell equations are solved on the basis of the Yee algorithm in discrete time and lattices.[40] FDTD is a dependable method to simulate a wide range of problems for electromagnetics, photonics, acoustics, and so on.[41] Using this method, the dynamics of light propagation and photon localization can be numerically simulated. To investigate laser dynamics, an auxiliary differential equation FDTD (ADE-FDTD) method has also been developed, in which the FDTD method is coupled with the classical electron oscillator model and the rate equation in a four-level energy system.[46-50] The ADE-FDTD method can simulate light emission from a photonic crystal, such as a defect mode laser or band edge laser.

We here consider light propagation in an active gain medium which induces a polarization. The Maxwell equations are written as

$$\nabla \times \mathbf{E} = -\mu_0 \frac{\partial \mathbf{H}}{\partial t} \tag{7}$$

$$\nabla \times \mathbf{H} = -\varepsilon_0 \varepsilon \frac{\partial \mathbf{E}}{\partial t} + \frac{\partial \mathbf{P}}{\partial t} \quad , \tag{8}$$

where **P** is a macroscopic polarization. On the basis of a classical electron oscillator model, the polarization **P** for an isotropic medium can be described by

$$\frac{\partial^2 P}{\partial t^2} + \Delta\omega_a \frac{\partial P}{\partial t} + \omega_a^2 P = \frac{\gamma_r}{\gamma_c} \frac{e^2}{m} \Delta N E \quad , \tag{9}$$

where $\Delta\omega_a = 1/\tau_{21} + 2/T_2$ is the full width at half maximum linewidth of atomic transition. T_2 is the mean time between dephasing events which is taken to be 5.0×10^{-15} s. $\Delta N(z,t) = N_1(z, t) - N_2(z, t)$ and $\gamma_r = 1/\tau_{21}$ is the real decay rate of the second level, and γ_c is the classical rate.

In a four-level atomic system, the rate equations are expressed as follows:

$$\frac{dN_3(z,t)}{dt} = P_r N_0(z,t) - \frac{N_3(z,t)}{\tau_{32}} \tag{10}$$

$$\frac{dN_2(z,t)}{dt} = \frac{N_3(z,t)}{\tau_{32}} + \frac{E(z,t)}{\hbar\omega_a}\frac{dP(z,t)}{dt} - \frac{N_2(z,t)}{\tau_{21}} \tag{11}$$

$$\frac{dN_1(z,t)}{dt} = \frac{N_2(z,t)}{\tau_{21}} - \frac{E(z,t)}{\hbar\omega_a}\frac{dP(z,t)}{dt} - \frac{N_1(z,t)}{\tau_{10}} \tag{12}$$

$$\frac{dN_0(z,t)}{dt} = \frac{N_1(z,t)}{\tau_{20}} - P_r N_0(z,t) \quad , \tag{13}$$

where N_0, N_1, N_2, and N_3 are the electron numbers at each energy level. The lifetimes at each energy level, τ_{32}, τ_{21}, and τ_{10}, are chosen to be 1×10^{-13}, 1×10^{-9}, and 1×10^{-11} s, respectively, and are similar to those of laser dyes such as coumarine or rhodamine. The total electron density $N_0^0 = N_0 + N_1 + N_2 + N_3$ is $5.5\times6.02\times10^{23}$, and initially, all of them are at the ground state ($N_0 = N_0^0$). Pumping rate P_r is a controlled variable that should be tuned by the pumping intensity in the real experiment.

In Fig. 12(a), the solid line is the calculated emission spectrum of a dye in bulk at a low pump rate by the ADE-FDTD method. The center wavelength of the dye spectrum is 570 nm and the half width at half maximum is 65 nm. The broken line is the transmission spectrum of a 1D photonic crystal without a defect. The physical properties of the 1D photonic crystal are as follows: $n_1 = 1.5$, $n_2 = 1.65$; $L_1 = 100$ nm, $L_2 = 100$ nm; and the number of layers is 20. Figure 12(b) shows the calculated dye emission spectra from the 1D photonic crystal without a defect as a function of pumping rate, where the spatial distribution of the dye is assumed to be uniform in the 1D photonic crystal. At a low pumping rate of 1×10^{10}, a broad spectrum is observed in which light emissions are suppressed by the photonic band. With increasing pumping rate, the spectral peak becomes higher and narrower at the band edge wavelength. Above a threshold, the single narrow peak appears at the band edge wavelength. There is a threshold at approximately a pumping rate of 1.5×10^{11}. Thus, the ADE-FDTD simulation has been a powerful tool because it can reproduce emission spectra and provide a laser threshold.

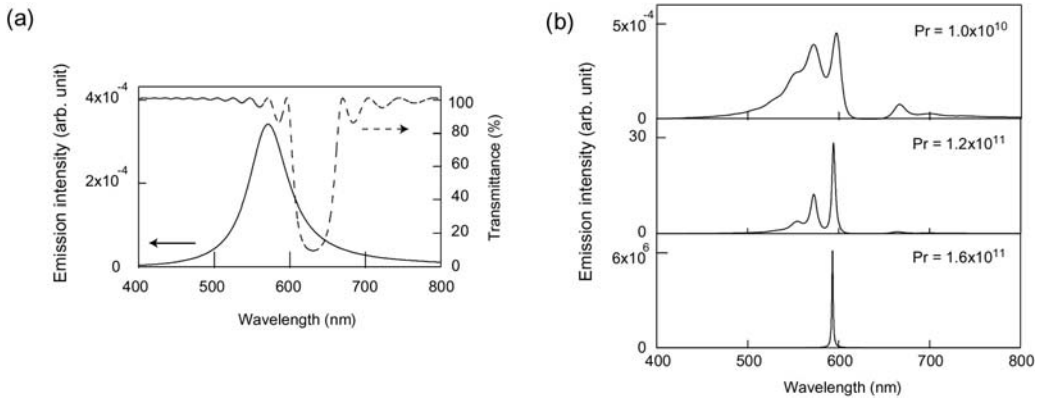

Fig. 12 ADE-FDTD simulation results: (a) Emission spectrum of a dye in ~~a~~ bulk and transmission spectrum of a 1D photonic crystal and (b) Emission spectra of a dye-doped 1D photonic crystal as a function of pumping rate.

4. Summary

We experimentally and theoretically studied the 1D photonic crystal with a liquid crystal defect layer for application as a tunable laser. Using field-induced liquid-crystal reorientation, the laser wavelength was able to be tuned with a low voltage. The photon confinement in the photonic crystal was discussed by calculating DOS. The confinement at defect mode was much stronger than that at band-edge mode. Furthermore, the emission spectra from the 1D photonic crystal were also simulated by the ADE-FDTD method. We expect that our proposed tunable system contributes for the development of new photonic crystal applications.

References

[1] P.G. de Gennes and J. Port, The Physics of Liquid Crystals, Oxford University Press, 1995.

[2] S. Chandrasekhar, Liquid Crystals, Cambridge University Press, 1992.

[3] H. Kawamoto, Proceedings of the IEEE, **90**, pp.460 - 500, 2002.

[4] D.K. Yang and S.T. Wu, Fundamentals of Liquid Crystal Devices, Wiley, 2006.

[5] K. Yoshino, Y. Shimoda, Y. Kawagishi, K. Nakayama, and M. Ozaki, Appl. Phys. Lett., **75**, pp.932 - 934, 1999.

[6] K. Yoshino, S. Satoh, Y. Shimoda, Y. Kawagishi, K. Nakayama, and M. Ozaki, Jpn. J. Appl. Phys., **38**, pp.L961 - L963, 1999.

[7] S.W. Leonard, J.P. Mondia, H.M. van Driel, O. Toader, S. John, K. Busch, A. Birner, U. Gösele, and V. Lehmann, Phys. Rev. B, **61**, pp.R2389 - R2392, 2000.

[8] R. Ozaki, T. Matsui, M. Ozaki, and K. Yoshino, Appl. Phys. Lett., **82**, pp.3593 - 3595, 2003.

[9] B. Maune, M. Lončar, J. Witzens, M. Hochberg, T. Baehr-Jones, D. Psaltis, A. Scherer, and Y. Qiu, Appl. Phys. Lett., **85**, pp.360 - 362, 2004.

[10] T.S. Perova, V.A. Tolmachev, E.V. Astrova, Y.A. Zharova, and S.M. O'Neill, Physica Status Solidi (c), **4**, pp.1961 - 1965, 2007.

[11] R. Ozaki, T. Shinpo, K. Yoshino, M. Ozaki, and H. Moritake, Appl. Phys. Express, **1**, pp.012003-1 - 012003-3, 2008.

[12] E. Yablonovitch, Phys. Rev. Lett., **58**, pp.2059 - 2062, 1987.

[13] S. John, Phys. Rev. Lett., **58**, pp.2486 - 2489, 1987.

[14] J.D. Joannopoulos, P.R. Villeneuve, and S. Fan, Solid State Communications, **102**, pp.165 - 173, 1997.

[15] K. Sakoda, Optical Properties of Photonic Crystals, Springer, 2005.

[16] A. Mekis, J. C. Chen, I. Kurland, S. Fan, P.R. Villeneuve, and J.D. Joannopoulos, Phys. Rev. Lett., **77**, pp.3787 - 3790, 1996.

[17] J.D. Joannopoulos, P.R. Villeneuve, and S. Fan, Nature, **386**, pp.143 - 149, 1997.

[18] K. Srinivasan and O. Painter, Opt. Express, **10**, pp.670 - 684, 2002.

[19] Y. Akahane, T. Asano, B.-S. Song, and S. Noda, Nature, **425**, pp.944 - 947, 2003.

[20] J.P. Dowling, M. Scalora, M.J. Bloemer, and C.M. Bowden, J. Appl. Phys., **75**, pp.1896 - 1899, 1994.

[21] O. Painter, R. K. Lee, A. Scherer, A. Yariv, J.D. O'Brien, P.D. Dapkus, and I. Kim, Science, **284**, pp.1819 - 1821, 1999.

[22] K. Sakoda, K. Ohtaka, and T. Ueta, Opt. Express, **4**, pp.481 - 489, 1999.

[23] M. Ozaki, M. Kasano, D. Ganzke, W. Haase, and K. Yoshino, Adv. Mater., **14**, pp.306 - 309, 2002.

[24] M. Ozaki, M. Kasano, T. Kitasho, D. Ganzke, W. Haase, and K. Yoshino, Adv. Mater., **15**, pp.974 - 977, 2003.

[25] H. Finkelmann, S.T. Kim, A. Muñoz, P. Palffy-Muhoray, and B. Taheri, Adv. Mater., **13**, pp.1069 - 1072, 2001.

[26] A. Chanishvili, G. Chilaya, G. Petriashvili, R. Barberi, R. Bartolino, G. Cipparrone, A. Mazzulla, and L. Oriol, Adv. Mater., **16**, pp.791 - 795, 2004.

[27] Y. Inoue, H. Yoshida, K. Inoue, Y. Shiozaki, H. Kubo, A. Fujii, and M. Ozaki, Adv. Mater., **23**, pp.5498 - 5501, 2011.

[28] H. Takeda and K. Yoshino, Phys. Rev. B, **67**, pp.073106-1 - 073106-4, 2003.

[29] S.Y. Lin, J.G. Fleming, D.L. Hetherington, B.K. Smith, R. Biswas, K.M. Ho, M.M. Sigalas, W. Zubrzycki, S.R. Kurtz, and J. Bur, Nature, **394**, pp.251 - 253, 1998.

[30] A. Blanco, E. Chomski, S. Grabtchak, M. Ibisate, S. John, S. W. Leonard, C. Lopez, F. Meseguer, H. Miguez, J.P. Mondia, G. A. Ozin, O. Toader, and H.M. Driel, Nature, **405**, pp.437 - 440, 2000.

[31] S. Noda, K. Tomoda, N. Yamamoto, and A. Chutinan, Science, **289**, pp.604 - 606, 2000.

[32] H.B. Sun, S. Matsuo, and H. Misawa, Appl. Phys. Lett., **74**, pp.786 - 788, 1999.

[33] J.S. Foresi, P.R. Villeneuve, J. Ferrera, E.R. Thoen, G. Steinmeyer, S.Fan, J.D. Joannopoulos, L.C. Kimerling, H.I. Smith and E.P. Ippen, Nature, **390**, pp.143 - 145, 1997.

[34] M. Notomi, E. Kuramochi, and H. Taniyama, Opt. Express, **16**, pp.11095 - 11102, 2008.

[35] M.D. Tocci, M.J. Bloemer, M. Scalora, J.P. Dowling, and C.M. Bowden, Appl. Phys. Lett., **66**, pp.2324 - 2326, 1995.

[36] T. Hattori, N. Tsurumachi, and H. Nakatsuka, J. Opt. Soc. Am., **14**, pp.348 - 355, 1997.

[37] Y. Dumeige, P. Vidakovic, S. Sauvage, I. Sgnes, and J. A. Levenson, Appl. Phys. Lett., **78**, pp.3021 - 3022, 2001.

[38] K.M. Ho, C.T. Chan, and C.M. Soukoulis, Phys. Rev. Lett., **65**, pp.3152 - 3155, 1990.

[39] M. Plihal and A.A. Maradudin, Phys. Rev. B, **44**, pp.8565 - 8571, 1991.

[40] K. S. Yee, IEEE Trans. on Antennas and Propagation, **45**, pp.354 - 363, 1966.

[41] A. Taflove and S. C. Hagness, Computational Electrodynamics: The Finite-Difference Time-Domain Method, 3rd ed., Artech House, 2005.

[42] D.W. Berreman, J. Opt. Soc. Am., **62**, pp.502 - 510, 1971.

[43] R. Ozaki, Y. Matsuhisa, M. Ozaki, and K. Yoshino, Appl. Phys. Lett., **84**, pp.1844 - 1846, 2004.

[44] J. M. Bendickson, J. P. Dowling, and Michael Scalora, Phys. Rev. E, **53**, pp.4107 - 4121, 1996.

[45] J. Schmidtkea and W. Stille, Eur. Phys. J. B, **31**, pp.179 - 194, 2003.

[46] A. S. Nagra and R. A. York, IEEE Trans. on Antennas and Propagation, **46**, pp.334 - 340, 1998.

[47] X. Jiang and C. M. Soukoulis, Phys. Rev. Lett., **85**, pp.70 - 73, 2000.

[48] S.-H. Chang and A. Taflove, Opt. Express, **12**, pp.3827 - 3833, 2004.

[49] S. Shi and D. W. Prather, Opt. Express, **15**, pp.10294 - 10302, 2007.

[50] T. Matsui and M. Kitaguchi, Appl. Phys. Express, **3**, pp.061701-1 - 061701-3, 2010.